Sliding Mode and PID Control of a Dual Stage Actuator for Precision Positioning

Shingo Ito   Juergen Steininger   Georg Schitter

Automation and Control Institute (ACIN), Vienna University of Technology, Gusshausstrasse 27-29, 1040, Vienna, Austria (e-mail: {ito, juergen.steininger, schitter}@acin.tuwien.ac.at)

Abstract: Actuators composing dual stage actuation usually have different purposes and mechanisms to complement each other. Hence, they potentially have different types of control challenges to achieve high-precision motion performance. This paper presents the use of single-input single-output controllers to efficiently overcome the potential problems by selecting proper control techniques to each actuator. The setup is a low-stiffness dual stage actuator capable of positioning with nanometer resolution without additional vibration isolation. The system consists of a CD/DVD laser pickup and a linear motor with roller bearings, which suffer from environmental vibrations and friction, respectively. By selecting and implementing a tamed PID controller for the pickup and a sliding mode controller for the linear motor, the dual stage actuator is able to move over $100\,\mathrm{mm}$ with a maximum velocity of $0.34\,\mathrm{m/s}$ and position with a static precision of $\pm\,2.5\,\mathrm{nm}$ (peak-to-peak).

1. INTRODUCTION

In applications where high-precision positioning over a long range is required, a single actuator may not be able to achieve the desired performance. To satisfy the requirements, a long-stroke coarse actuator can be combined with a short-stroke fine (high-precision) actuator as a dual stage actuator (DSA). This technique has been successfully applied to many applications, such as optical disk drives (Chaghajerdi [2008]) and wafer scanners for lithography (Butler [2011]).

In order to control DSA systems, multi-input multi-output (MIMO) control design can be applied, since they can be regarded as a system with at least multiple inputs. The MIMO control includes H_2 control, H_∞ control, μ-synthesis, and sliding mode control (SMC) (Hu et al. [1998], Al Mamun et al. [2003], Tai and Chen [2005], Nagamune et al. [2006]). These controls can guarantee the stability and robustness of the overall system. Another strategy to control DSA systems is to design single-input single-output (SISO) controllers for the fine and coarse actuators in a certain configuration (Guo et al. [1999]). By using the SISO control design, the order of controllers can be lower than that of MIMO (Semba et al. [1999]). More importantly, the SISO design has the freedom of selecting the control design techniques individually for the fine actuator and the coarse actuator, whereas the MIMO usually applies same techniques to both. In fact, Herrmann et al. [2007] successfully applied discrete SMC to the fine actuator, while using proximate time-optimal control for the coarse actuator in a hard disk drive (HDD).

In general, the fine actuator and the coarse actuator of a DSA have different actuation principles and mechanisms to complement each other. For example, a piezoelectric stage is mounted onto a gantry stage with ball screws and DC servo motors to compensate for backlash and

friction (Lin et al. [2009]). A piezoelectric device is also installed as the fine actuator on a voice coil motor to increase the control bandwidth in a HDD. In a wafer scanner, short-stroke Lorentz actuators are used together with linear motors, physically isolating disturbances such as floor vibrations (Butler [2011]). Due to such multiple actuation principles potentially existing in a DSA system, it is natural that different types of control challenges arise individually for the fine actuator and the coarse actuator. To overcome such problems for high-precision positioning over a long range, the SISO control design can be effectively applied by utilizing the freedom of control technique selection. In other words, the SISO design allows the user to pick proper tools to individually solve the distinct control problems.

This paper presents a low-stiffness DSA, which is constructed to achieve long-range positioning with nanometer resolution without extra vibration isolation (e.g. an optical table) (Ito et al. [2013]). This system consists of a laser pickup of a CD/DVD player as the fine actuator and a linear motor with roller bearings as the coarse actuator. For these actuators, controllers are individually designed to achieve high-speed high-precision positioning over a long range.

The rest of this paper is organized as follows. Section 2 introduces the DSA system. This system is modeled and its disturbances are analyzed in Section 3. Controllers are designed in Section 4. Section 5 presents experimental results, comparing performance of the SISO control design with and without the individual control technique selection. The paper is concluded in Section 6.

2. SYSTEM DESCRIPTION

Fig. 1 shows a DSA setup built on a pick-and-place machine (CAT(2a), Philips, Amsterdam, Netherlands), with-
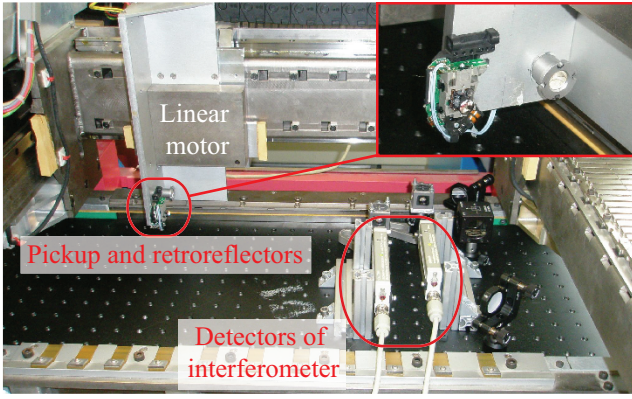
Fig. 1. Photograph of the DSA setup.

out external vibration isolation such as an optical table. This machine has six linear motors, and one of them is used as the long-stroke coarse actuator of the DSA. The linear motor is guided by roller bearings and operated by a servo driver in force control mode. As the fine actuator, a Lorentz actuator in a laser pickup (SF-HD65, Sanyo, Osaka, Japan) is used and driven by a voltage amplifier. The actuation range of the fine actuator is limited to approximately $\pm 1\,\mathrm{mm}$. To optically measure the fine actuator position, its objective lens is replaced by a cube-corner retroreflector, and an interferometer (10899A, Agilent Technologies, San Francisco, USA) is mounted on the platform for the real time control of the DSA. The interferometer has a resolution of $1.25\,\mathrm{nm}$ and detects movement up to $0.40\,\mathrm{m/s}$. An additional retroreflector is mounted on the coarse actuator to measure its position with a second interferometric detector. This second sensor is not used for the control, but for evaluation only.

The servo driver, the voltage amplifier and the interferometers are all connected to a rapid control prototyping system (DS1005(CPU), DS5203(FPGA), DS2102(DAC), dSpace GmbH, Paderborn, Germany), where controllers are implemented running at a sampling frequency of $20\,\mathrm{kHz}$. This system is also used for data acquisition.

3. SYSTEM ANALYSIS

3.1 Dynamic model

Fig. 2 shows a lumped mass model of the DSA setup, where x_f and x_c are the positions of the fine and coarse actuators, respectively. Their forces are expressed as F_f and F_c, and k and c are the stiffness and damping of the fine actuator. The moving mass of the fine actuator with the retroreflector is m_f and is about $0.7\,\mathrm{g}$. The total mass of the coarse actuator's moving part including the stator of the fine actuator is m_c, and it is approximately $8.5\,\mathrm{kg}$. To relate the actuator forces with the actuator drivers, two constants K_{af} and K_{ac} are introduced as

$$F_f = K_{af}u_f, \qquad F_c = K_{ac}u_c, \qquad (1)$$

where u_f and u_c are the reference inputs of the drivers for the fine and coarse actuation, respectively. Using these inputs, the actuator positions can be expressed in the following equations under an assumption that m_c is sufficiently larger than m_f (Ito et al. [2013]):

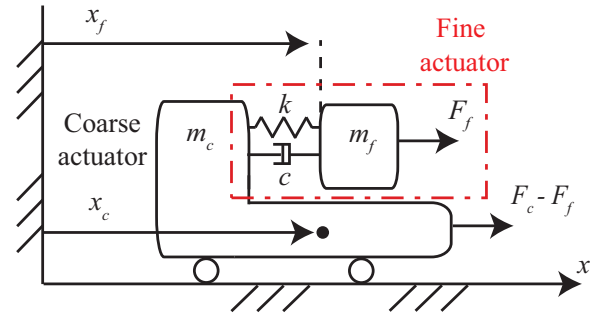$$X_f(s) = P_f(s)(K_{af}U_f(s) + P_d(s)X_c(s)), \qquad (2)$$

Fig. 2. Lumped mass model of DSA.

$$X_c(s) = P_c(s)K_{ac}U_c(s), \qquad (3)$$

where $X_f(s)$, $X_c(s)$, $U_f(s)$ and $U_c(s)$ are the Laplace transformations of x_f, x_c, u_f and u_c, respectively. $P_f(s)$ and $P_c(s)$ are transfer functions that dominate the fine and coarse actuation, and $P_d(s)$ represents the mechanical coupling of the two actuators. These transfer functions are given as

$$P_f(s) = X_f(s)/F_f(s) = (m_f s^2 + cs + k)^{-1}, \qquad (4)$$

$$P_c(s) = X_c(s)/F_c(s) = (m_c s^2)^{-1}, \qquad (5)$$

$$P_d(s) = cs + k. \qquad (6)$$

3.2 Parameter estimation

The unknown parameters in Section 3.1 are estimated by measuring corresponding frequency response data and fitting a model. Fig. 3 shows a Bode plot of the fine actuator and the fitting result using the fine actuator model $K_{af}P_f(s)$. The model shows a good fit at least up to $1\,\mathrm{kHz}$. It does not capture the second mechanical resonance at a relatively high frequency (around $6\,\mathrm{kHz}$) to keep its order low. Additional phase lag at high frequencies ($> 10\,\mathrm{kHz}$) is due to a pole created by the resistance and inductance of the pickup's coil. Because the current through the coil is proportional to its voltage up to these high frequencies, a voltage amplifier is used for the fine actuator as mentioned.

A Bode plot of the coarse actuator and curve fitting based on the course actuator model $K_{ac}P_c(s)$ are shown in Fig. 4, where the dynamic system is well captured approximately up to $100\,\mathrm{Hz}$. A mechanical resonance at about $240\,\mathrm{Hz}$ is not modeled to keep the model simple for control design. The estimated parameters are listed in Table 1.

Table 1. Estimated parameters

Parameter	Value	Unit
k	42	N/m
c	3.5×10^{-2}	N/(m/s)
K_{af}	2.59×10^{-2}	N/V
K_{ac}	51	N/V

3.3 Disturbance of fine actuation

To achieve high-precision positioning with nanometer resolution at static positions, the fine actuator needs to reject environmental vibrations. For the evaluation of the disturbances to be rejected by the fine actuator, its position x_f is measured while both actuators are turned off. The measured positional data in the time domain and the frequency
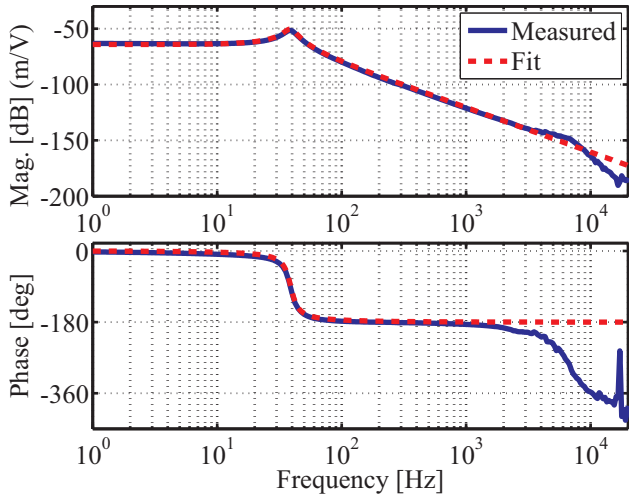
Fig. 3. Bode plot of fine actuator (blue solid line) and curve fitting result (red dashed line).
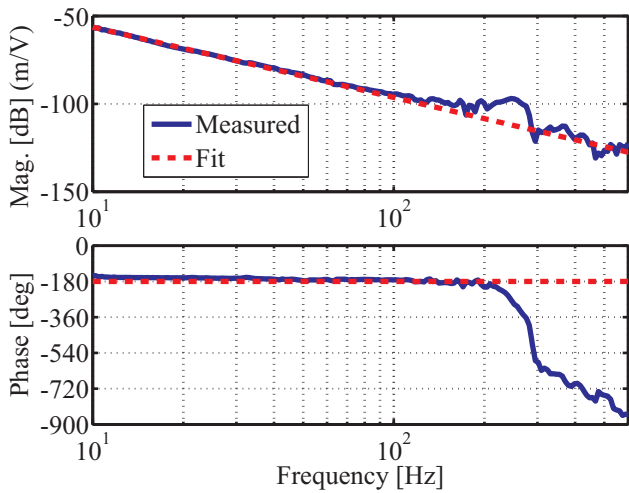

Fig. 4. Bode plot of coarse actuator (blue solid line) and curve fitting result (red dashed line).

domain are shown in Fig. 5. The spectrum analysis shows that the major frequency components are below 80 Hz.

3.4 Disturbance of coarse actuation

For high-precision positioning, the fine actuator follows the position reference. Meanwhile, the coarse actuator carries the stator of the fine actuator, such that the coil of the fine actuator always stays within its uniform magnetic field. By doing so, the fine actuator can be operated in its linear range over the full DSA stroke. Therefore, to achieve high-speed positioning, the coarse actuator needs to move fast enough, while its accuracy can be as poor as submillimeters for the fine actuator stroke (± 1 mm). For this reason, the major disturbance of the coarse actuator is friction due to the roller bearings, rather than the environmental vibrations.

Friction can be described as a combination of the static, Coulomb and viscous model (Armstrong-Hélouvry et al. [1994]). To evaluate the roller bearings, it is presumed that its viscous friction is not a major disturbance source, as damping effects cannot be obviously seen in Fig. 4.
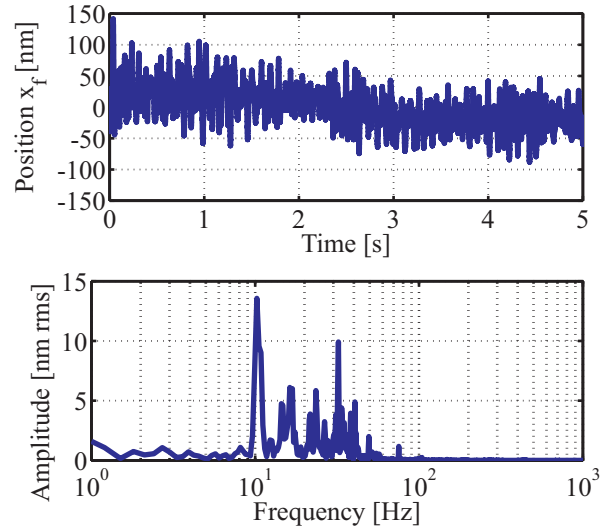

Fig. 5. Fine actuator position x_f (top) and its power spectrum (bottom) while both actuators are disabled.

Thus, the maximum friction is measured as the force required to start rolling the bearing balls. This required force is externally applied and measured by a sensor (FSG-15N1A, Honeywell, New Jersey, USA). The measurement is conducted 50 times at different positions. The results show that the friction depends on the coarse actuator position and varies between 8.2 N and 25.9 N. The mean value of the 50 measurements is 18.5 N. The measured maximum friction is considered at the controller design in Section 4.3.

4. CONTROLLER DESIGN

4.1 Observer

As mentioned in Section 2, only the fine actuator position x_f is measured for the real time control. To regulate the coarse actuator, its velocity and position are estimated by a Kalman filter. The Kalman filter is designed based on a state-space model corresponding to (2) and (3), that is

$$\dot{x}_{ss} = Ax_{ss} + Bu_{ss}, \qquad y = Cx_{ss}, \qquad (7)$$

using

$$x_{ss} = [\, x_f \ x_c \ \dot{x}_f \ \dot{x}_c \,]^T, \qquad u_{ss} = [\, u_f \ u_c \,]^T,$$

$$A = \begin{bmatrix} 0 & 0 & 1 & 0 \\ 0 & 0 & 0 & 1 \\ -k/m_f & k/m_f & -c/m_f & c/m_f \\ 0 & 0 & 0 & 0 \end{bmatrix},$$

$$B = \begin{bmatrix} 0 & 0 \\ 0 & 0 \\ K_{af}/m_f & 0 \\ 0 & K_{ac}/m_c \end{bmatrix}, C = [\, 1 \ 0 \ 0 \ 0 \,], \quad (8)$$

where y is the output. Note that this model is observable if $k \neq 0$. In the case of a zero-stiffness DSA (i.e. $k = 0$), an additional sensor is required for the DSA operation.

4.2 Feedback control of fine actuator

Since the fine actuator has the first mechanical resonance at a low frequency and shows a phase of $-180°$ up to high frequencies in Fig. 3, its feedback controller should provide
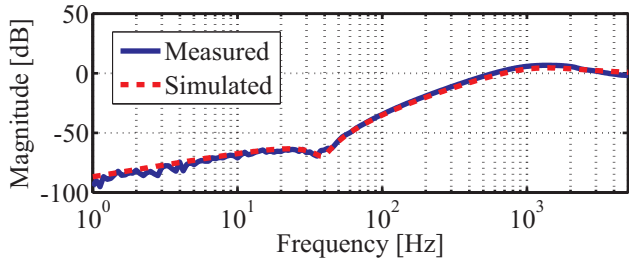
Fig. 6. Measured (blue solid line) and simulated (red dashed line) sensitivity function of fine actuation.

a phase lead to achieve both high control bandwidth and good disturbance rejection. Furthermore, it is preferred that the controller is low order for the simplicity of implementation. Therefore, a PID controller with a low pass filter (tamed PID) is selected for the fine actuation (Munnig Schmidt et al. [2011]). This controller is tuned based on the fine actuator model $K_{af}P_f(s)$, such that its open-loop crossover frequency is $1\,\mathrm{kHz}$ with a sufficient phase margin. Fig. 6 shows the sensitivity function of the closed-loop fine actuation.

Saturation can be a problem with short-stroke actuators, where anti-windup control can improve stability (Kong et al. [2010]). For precision positioning, however, the saturation has to be avoided by keeping the fine actuator within its linear operation range, which requires an according control of the coarse actuator (cf. Fig. 9).

4.3 Feedback control of coarse actuator

For the coarse actuation, SMC is used as the feedback controller to compensate for the friction. SMC is nonlinear control and has an excellent performance on disturbance rejection. Particularly when the matching condition is satisfied, the closed-loop system can be invariant to the disturbances in ideal cases. Moreover, the controller design requires only the upper bound of the disturbances. In this section, the SMC design is divided into three steps: augmentation of the coarse actuator model, switching surface design based on the behavior of the system in the sliding mode, and control input design to enforce the sliding mode (Shtessel et al. [2013]).

The design of SMC is discussed based on Fig. 7, which shows the coarse actuator model and the SMC structure for the design. First of all, the coarse actuator model $P_c(s)$ with K_{ac} is described as a state-space model with the friction force as disturbance d_c:

$$\dot{x}_{c\_ss} = A_c x_{c\_ss} + B_{cu} u_c + B_{cd} d_c, \qquad (9)$$

using

$$x_{c\_ss} = \begin{bmatrix} x_c & \dot{x}_c \end{bmatrix}^T,$$

$$A_c = \begin{bmatrix} 0 & 1 \\ 0 & 0 \end{bmatrix}, B_{cu} = \begin{bmatrix} 0 \\ K_{ac} m_c^{-1} \end{bmatrix}, B_{cd} = \begin{bmatrix} 0 \\ m_c^{-1} \end{bmatrix}, \quad (10)$$

For the SMC design, this state-space model is augmented with an integrator and a low pass filter (LPF). The integrator integrates the tracking error e_c of the coarse actuation. By incorporating this integrator, the coarse actuator is able to track its reference r_c without a steady-state error. The LPF is added as a prefilter of the coarse actuator to mitigate the chattering phenomenon by attenuating unmodeled mechanical resonances (Ito and Nonami

[1997]). Since the first unmodeled mechanical resonance is around $240\,\mathrm{Hz}$ in Fig 4, its cutoff frequency should be sufficiently lower than the resonant frequency. Thus, the LPF is designed, such that its cutoff frequency is $70\,\mathrm{Hz}$, and is implemented in the form of a second-order state-space model as shown in Fig. 7. For the SMC design, the augmented model is expressed in the following state equation:

$$\dot{x}_{a\_ss} = A_a x_{a\_ss} + B_{a\_u} u_a + B_{a\_r} r_c + B_{a\_d} d_c, \qquad (11)$$

where x_{a_ss} is a $5{\times}1$ state vector.

As the second step of the design, a linear switching surface is introduced as the following manifold:

$$\sigma(x_{a\_ss}) = S x_{a\_ss} = 0, \qquad (12)$$

where S is a $1{\times}5$ matrix. While the system is forced to the sliding mode, $\sigma = 0$ and $\dot{\sigma} = 0$ are satisfied. Using the latter condition and (11) with $d_c = 0$, the equivalent control u_{eq} can be obtained as

$$u_{eq} = -(SB_{a\_u})^{-1}(SA_a x_{a\_ss} + SB_{a\_r} r_c). \qquad (13)$$

Substitution of (13) for the control input of (11) with $d_c = 0$ yields the system motion restricted to the switching surface:

$$\dot{x}_{a\_ss} = (I - B_{a\_u}(SB_{a\_u})^{-1}S)(A_a x_{a\_ss} + B_{a\_r} r_c). \quad (14)$$

By selecting x_c as the output of (14), the control bandwidth of the system during the sliding mode can be obtained from the frequency response from r_c to x_c. Matrix S is determined, such that the control bandwidth is around $15\,\mathrm{Hz}$, which corresponds to the bandwidth achieved by a lead-lag compensator for benchmarking (Section 4.5).

As the third step of the design, the control input u_a is selected as a combination of the equivalent control (13) and a switching control u_{sw}:

$$u_a = u_{eq} + u_{sw}. \qquad (15)$$

u_{sw} enforces the sliding mode to the system and is composed of a relay with a gain and a linear continuous feedback as it follows:

$$u_{sw}(\sigma(x_{a\_ss})) = -k_{sw1}sgn(\sigma(x_{a\_ss})) - k_{sw2}\sigma(x_{a\_ss}), \quad (16)$$

where k_{sw1} and k_{sw2} are constants. To determine their values, a Lyapunov function $V = \sigma^2/2$ is considered. For the existence and the stability of the sliding mode, the following equation needs to be satisfied:

$$\dot{V} = \sigma(x_{a\_ss})\dot{\sigma}(x_{a\_ss}) = \sigma(x_{a\_ss})S\dot{x}_{a\_ss} < 0. \qquad (17)$$

Using (11)(15)(16), (17) leads to the following satisfactory condition:

$$k_{sw1} + |\sigma(x_{a\_ss})|k_{sw2} > |(SB_{a\_u})^{-1}SB_{a\_d}||d_{c\_max}|, \quad (18)$$

where d_{c_max} is the maximum friction measured in Section 3.4. Finally, the relay function in (16) is smoothed by a sigmoid function, which prevents the chattering by restricting the system not to the switching surface (12), but to its neighborhood. The sigmoid parameter, k_{sw1} and k_{sw2} are fine-tuned at the controller implementation, satisfying (18).

4.4 Overall control of DSA

Fig. 8 shows overall control blocks of the DSA system. The DSA is decoupled by a prefilter $K_{af}^{-1}P_d(s)^{-1}$, and the designed SISO controllers are applied to the corresponding actuators. "Observer", "PID" and "SMC" blocks are the
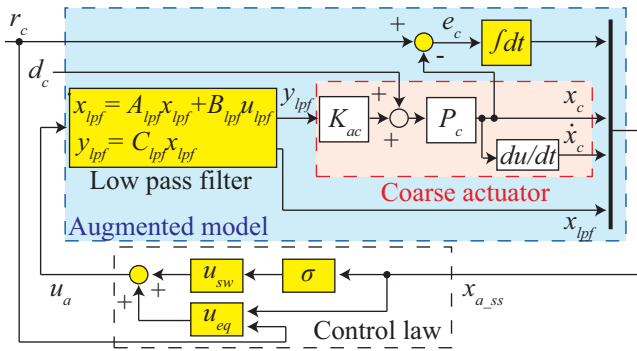
Fig. 7. Coarse actuator model and SMC structure for control design. The colored blocks are implemented in the "SMC" block of Fig. 8.
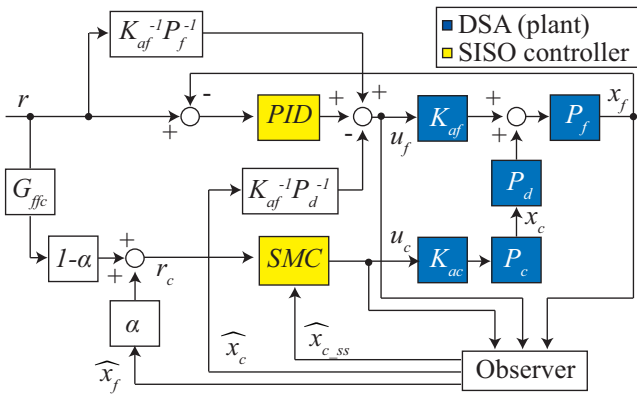

Fig. 8. Overall control block diagram of DSA.

Kalman filter, the tamed PID and the SMC presented in the previous sections, respectively. To achieve high-speed positioning to track the reference r, $K_{af}^{-1}P_f(s)^{-1}$ and $G_{ffc}(s)$ are added for feedforward control. $G_{ffc}(s)$ is an input-shaping filer and is the inverse of the transfer function obtained from (14) by selecting x_c as the output. To generate the coarse actuation reference r_c, a parameter α tunable between 0 and 1 is introduced. With $\alpha = 0$, the coarse actuator tracks r, while it follows the fine actuator (i.e. master-slave mode) by setting $\alpha = 1$. For experiments, α is set at 0.5 to a first approximation.

4.5 Controller for benchmarking

Benchmark controllers are designed for comparison. Although they use the same tamed PID for the fine actuator, a lead-lag compensator is used for the coarse actuation (cf. Ito et al. [2013]). The compensator is designed based on the coarse actuator model $K_{ac}P_c(s)$, and is fine-tuned to maximize its control bandwidth at the implementation, which is about 15 Hz. The DSA configuration is slightly different in that the master-slave control is used (α=1) with feedforward to the coarse actuator. Note that both feedback controllers are second-order filters in this benchmark system.

5. EXPERIMENTAL RESULTS

Positioning using a minimum jerk trajectory (Yamaguchi et al. [2011]) of 100 mm is conducted twice with the DSA system. The first experiment is relatively slow positioning
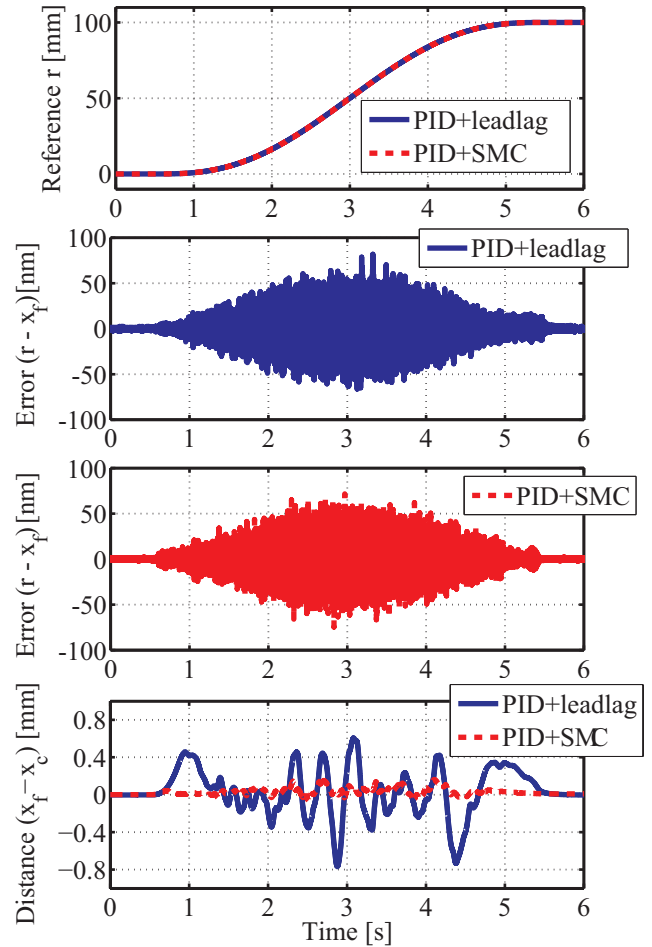

Fig. 9. Slow positioning of DSA. The first graph shows a reference. The second and third show a position error when a lead-lag compensator and SMC are used for the coarse actuation, respectively. The last compares the relative distance between the two actuators measured by the interferometers.

with a maximum velocity of 37.5 mm/s, and the results are shown in Fig. 9. The DSA position error $r - x_f$ is less than $\pm 100\,nm$ even during motion for the high disturbance rejection of the PID, and it does not show major difference between the two DSA systems. However, the relative distance between the two actuators measured by the two interferometers (i.e. $x_f - x_c$) is reduced by almost 80% by the use of SMC. The graph also shows that the relative distance of the benchmark controllers (PID+leadlag) is close to the stroke limit of the fine actuator (± 1 mm).

The second experiment is fast positioning with a maximum velocity of 0.34 m/s, which is 85% of the detectable velocity of the interferometers. Because the fine actuator reaches its stroke limit with the benchmark controllers, this experiment is conducted only for the DSA with the PID and SMC. The results are shown in Fig. 10, where the relative distance stays well within the ± 1 mm positioning range of the fine actuator. The settling time of the positioning over 100 mm to reach the ± 10 nm error band is only 0.6 s. The position error is well suppressed within the range of ± 2.5 nm before and after the positioning without an external vibration isolation.
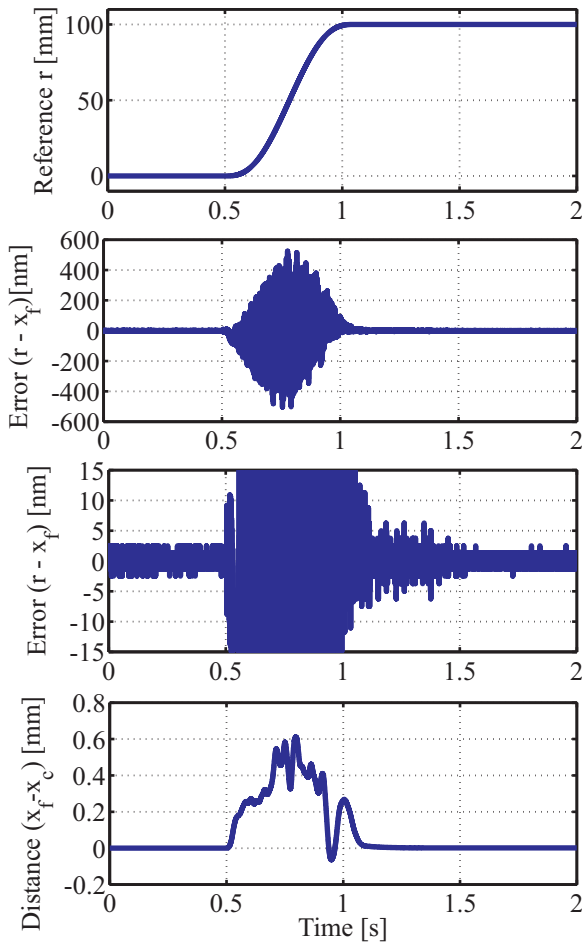
Fig. 10. Fast positioning of DSA using tamed PID and SMC. The first graph shows a reference. The second and third show a position error with different scales. The last shows the relative distance between the two actuators measured by the interferometers

6. CONCLUSION

In this paper a tamed PID and SMC have been individually designed and implemented for the fine and coarse actuators, respectively, to overcome the range and speed limitation due to friction and external disturbances in a DSA system. The experimental results show that the SMC of the coarse actuator reduces the relative distance between the fine and coarse actuator by almost 80% during motion as compared to the lead-lag controlled coarse actuator, which prevents the fine actuator from reaching its range limits during repositioning. As a result, the DSA controlled by the tamed PID and SMC is able to achieve a higher positioning speed while maintaining high precision without an additional vibration isolation system.

ACKNOWLEDGEMENTS

REFERENCES

A. Al Mamun, I. Mareels, T. H. Lee, and A. Tay. Dual stage actuator control in hard disk drive - a review. In *The 29th Annual Conference of the IEEE Industrial Electronics Society*, volume 3, pages 2132–2137, 2003.

B. Armstrong-Hélouvry, P. Dupont, and C. Canudas de Wit. A survey of models, analysis tools and compensation methods for the control of machines with friction. *Automatica*, 30(7):1083 – 1138, 1994.

H. Butler. Position control in lithographic equipment. *IEEE Control Systems Magazine*, 31(5):28 –47, 2011.

A.H. Chaghajerdi. Sensing and control in optical drives. *IEEE Control Systems Magazine*, 28(3):23 –29, 2008.

L. Guo, D. Martin, and D. Brunnett. Dual-stage actuator servo control for high density disk drives. In *IEEE/ASME International Conference on Advanced Intelligent Mechatronics*, pages 132 –137, 1999.

G. Herrmann, C. Edwards, B. Hredzak, V. Venkataramanan, and S.K. Spurgeon. Application of a discrete sliding mode technique to a hdd dual-stage track-seek and track-following servo system. In *IEEE 22nd International Symposium on Intelligent Control.*, pages 283–288, 2007.

X.P. Hu, S. Weerasooriya, T.S. Low, and B. M. Chen. Dual stage actuator modeling and control in a cd-rom drive. In *Proceedings of the 24th Annual Conference of the IEEE Industrial Electronics Society, 1998.*, volume 3, pages 1394–1398 vol.3, 1998.

S. Ito, J. Steininger, P. I. Chang, and G. Schitter. High-precision positioning system using a low-stiffness dual stage actuator. In *6th IFAC Symposium on Mechatronic Systems*, 2013.

T. Ito and K. Nonami. Sliding mode control with frequency shaping to suppress spillover (in Japanese). *Transactions of Japan Society of Mechanical Engineers*, 63(611):120–126, 1997.

K. Kong, H.C. Kniep, and M. Tomizuka. Output saturation in electric motor systems: identification and controller design. *Journal of Dynamic Systems, Measurement and Control*, 132:051002, 2010.

C.J. Lin, C.H. Wu, and C.C. Hwang. Tracking control of a motor-piezo XY gantry using a dual servo loop based on ILC and GA. In *IEEE International Conference on Control and Automation*, pages 1098 –1103, dec. 2009.

R. Munnig Schmidt, G. Schitter, and J. van Eijk. *The Design of High Performance Mechatronics*. Delft University Press, 2011.

R. Nagamune, Xinghui Huang, and R. Horowitz. Robust H2 synthesis for dual-stage multi-sensing track-following servo systems in HDDs. In *American Control Conference, 2006*, pages 1284–1289, 2006.

T. Semba, T. Hirano, J. Hong, and L.-S. Fan. Dual-stage servo controller for HDD using MEMS microactuator. *IEEE Transactions on Magnetics*, 35(5):2271 –2273, 1999.

Y. Shtessel, C. Edwards, L. Fridman, and A. Levant. *Sliding Mode Control and Observation*. Control Engineering. Birkhäuser, 2013.

Tsang-Li Tai and Jian-Shiang Chen. Discrete-time sliding-mode controller for dual-stage systems - a hierarchical approach. *Mechatronics*, 15(8):949 – 967, 2005.

T. Yamaguchi, M. Hirata, and C.K. Pang. *High-Speed Precision Motion Control*. Taylor & Francis, 2011.